actuators

MDPI

Article

Tele-Guidance of a Soft Magnetic Microrobot Transported by a Fluid in a Vascular Network

Ahmed Chah [1] and Karim Belharet [2,*]

[1] INSA-CVL/HEI Campus Centre, PRISME EA 4229, 36000 Châteauroux, France; ahmed.chah@junia.com
[2] JUNIA-HEI Campus Centre, PRISME EA 4229, 36000 Châteauroux, France
* Correspondence : karim.belharet@junia.com

Abstract: Electromagnetic actuation represents a novel wireless control approach utilized for the manipulation of magnetic microrobots, particularly in the context of diverse minimally invasive therapeutic applications. This study presented contributions relating to the integration of a human operator into the control system of an electromagnetic actuation framework through haptic assistance. The intervention of a human operator serves multiple purposes, encompassing the safe piloting of the microrobot during the procedure and the utilization of the doctor's expertise. Consequently, this human-in-the-loop approach not only ensures heightened safety but also enhances public acceptability, particularly in the realm of drug delivery within the human body. To facilitate these objectives, a haptic device was proposed to propel and orient the microrobots within blood vessels, thereby enabling their targeted delivery. Additionally, a novel magnetic guidance strategy was introduced, relying on the utilization of two magnetic forces to simplify and optimize the guidance process. The electromagnetic actuation system, developed in our research laboratory, offers a comprehensive workspace that has been obtained through analytical and quantitative modeling of the magnetic field generated by the system. With an accessible workspace encompassing a cubic volume of 70 mm in length, the system facilitates easy access from all four lateral sides. Such an architectural design allows for efficient manipulation of microparticles within a significantly larger 3D workspace, surpassing the limitations imposed by traditional systems primarily confined to a small central area, as observed in existing literature. Experimental evaluations encompassing both 2D and 3D scenarios were conducted to validate the efficacy of the magnetic navigation platform.

Keywords: haptic device; tele-operated system; electromagnet; actuation; microrobot

Citation: Chah, A.; Belharet, K. Tele-Guidance of a Soft Magnetic Microrobot Transported by a Fluid in a Vascular Network. *Actuators* **2023**, *12*, 283. https://doi.org/10.3390/act12070283

Academic Editors: Ignacio Valiente Blanco and Efren Diez-Jimenez

Received: 20 June 2023
Revised: 6 July 2023
Accepted: 10 July 2023
Published: 12 July 2023

1. Introduction

In recent years, as microrobots have begun to represent hope for the treatment of a significant number of diseases, the manipulation of medical microrobots has been the focus of attention of many scientists and researchers, especially after experiencing a massive development which shows progress in obtaining high efficacy of the remedies. Basically, the process is to guide and drive these microrobots (drug carriers) inside the body using a magnetic field. This technique is so precise that it not only allows the targeting of infectious regions, tumors, or any malignant tissue [1,2] that requires complex surgery, without affecting healthy organs as is the case with the traditional therapies. Therefore, the use of microrobots is minimally invasive [3–5] and more efficient [6,7]. However, to successfully implement this procedure, it is necessary to have a powerful electromagnetic actuation system with sufficient working space. In addition, a precise manipulation method would be required to effectively control the microrobot.

During the past years, several configurations of electromagnetic coils have been proposed for wireless actuation of microrobots [8–13]. The use of two coils makes it possible to produce a modular magnetic field by varying the electric current to manipulate and control the microrobots in the workspace located between the two coils. This consists of Helmholtz coils to generate a uniform magnetic field or Maxwell coils to produce a uniform magnetic gradient. Three pairs of Maxwell or Helmholtz coils arranged perpendicularly generate, respectively, a uniform magnetic field or gradient in 3D space [8]. Various electromagnetic systems have been proposed in the literature [10–14] with different characteristics in terms of electromagnet configuration, working space, and magnetic field distribution. The OctoMag [12] combines eight coils to generate a magnetic field and gradient capable of driving an intraocular microrobot in 5-DOF. It was designed for ophthalmic procedures like retinal-vein cannulation, with a semispherical accessible space of 130 mm diameter. An EMA system composed of five electromagnetic coils called the Mag-μBot was proposed in [15], offering an accessible space with a 3D volume of $100 \times 100 \times 100$ mm. An electromagnetic system that contained eight air-cor electromagnets was designed in [16], providing an accessible space of $120 \times 120 \times 120$ mm.

The use of these electromagnetic systems in automatic mode imposes some constraints. The first consists in obtaining a model of the dynamics of the microrobot in its environment and the latter is physiological, therefore very changing and variable; its modeling became very complex. Indeed, it is very difficult to obtain a precise model or exact physiological parameters, such as the blood velocity or the position of the blood vessel, for example. In automatic mode, it is also necessary to know in advance the trajectory that the microrobot must follow for the execution of automatic mode in a closed loop. The planning of this trajectory is very complex, especially in the context of navigation in the human vascular network. The other constraint in the execution of the automatic mode is access to the position of the microrobot in real time to ensure controller convergence. Indeed, obtaining the 3D position of the microrobot from clinical images would require robust image processing algorithms which generally require a very large calculation time. For these different constraints, automating the navigation of the microrobot in any drug targeting application may not be the best solution from an application point of view.

That is why we need a human operator in the control loop to eliminate all doubts that could cause the loss of the microrobot inside the human body. This intervention of a human operator is not only helpful to ensure secured steering of the microrobot during the process but it can also be beneficial to have all the expertise of a doctor, which would be a lot more responsible, safe, and even acceptable to the public as a system for drug delivery applications to a human body [17]. In such a case, integrating a haptic device in a teleoperated system can make the interaction with the distant environment more sensible and natural during manipulation. So, different from contact-based micro-manipulations, studies carried out to develop haptic feedback in non-contact micro-manipulations are rare. From this standpoint, a recent scientific investigation [18] aimed to elucidate a navigation approach by employing a haptic system for deflecting a microrobot at bifurcations and exploiting hydrodynamic force as the propulsive mechanism to guide the microrobot towards the branching point. A two-dimensional vascular network was employed as the experimental model, wherein a uniaxial actuation system encompassing two coils in the z-axis generated the magnetic force, and a haptic joystick facilitated the directional manipulation of the magnetic force, either upward or downward. Consequently, the authors' proposed navigation strategy involved maneuvering the microrobot towards the bifurcation, thereby directing it towards the intended branch. Nonetheless, given that the conducted tests were conducted under simplified circumstances, it is crucial to assess the efficacy of this strategy within a complex vascular network representative of realistic conditions. Furthermore, although the utilization of hydrodynamic force is intriguing, employing magnetic flux lines would be more favorable for ensuring precise control of the microrobot while minimizing the required magnetic energy. The non-contact systems that already exist with haptic feedback are mostly on magnetic tweezers and optical tweezers [19–22]; however, the other non-contact systems that focus on drug delivery using magnetic microrobots function only on 1D or 2D. Equally important, to improve human performance in remotely manipulated tasks, there is a process of transferring a block of program code into internal memory to provide navigation information in teleoperation to assist the operator [23]. This process can be executed by virtual fixtures known as active constraints. In essence, "virtual fixtures" are software-generated force and position signals adjusted to human operators, such as doctors in our case, to improve the safety, precision, performance, and agility of microrobot assisted manipulation tasks [24–26]. Virtual fixtures are efficient and intuitive because they have an advantage from both the perfection of robotic systems and the intellect of human operators.

In this work, As presented in the Figure 1, we proposed a navigation strategy for microrobots that utilizes a haptic device to control the magnetic force generated by a magnetic actuation system. This approach leverages magnetic flux lines to facilitate navigation and reduce energy consumption. The aim was to integrate clinicians' knowledge and expertise into the procedure, particularly their precise understanding of vascular anatomy. Their involvement enables accurate and safe navigation of microrobots within vascular networks. Our method avoids the use of closed-loop controls, eliminating the need for complex and unstable models associated with physiological parameters. By simplifying the navigation process, our approach offers a more practical and efficient implementation.

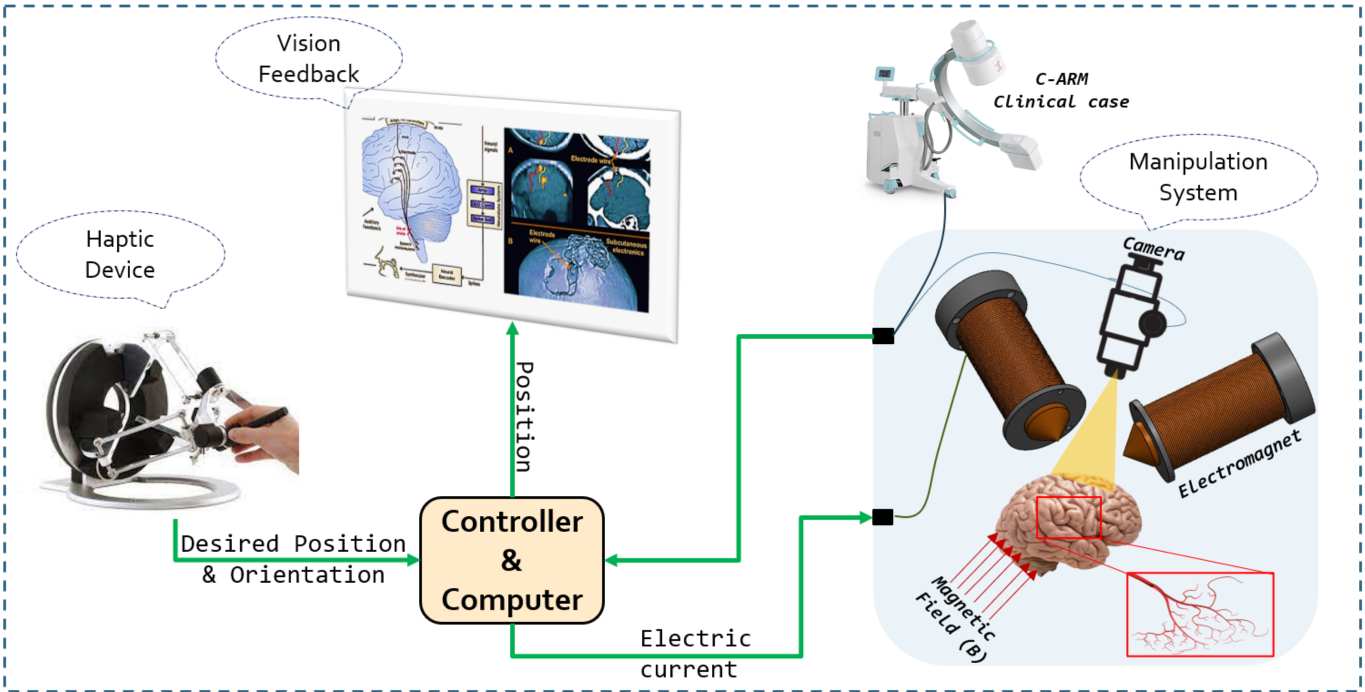

Figure 1. Conceptual diagram of the whole control system.

2. Navigation Strategy and Modeling

In our approach, we proposed harnessing the hydrodynamic force induced by the circulating flow to propel a spherical microrobot from its injection point to a specific target zone. Once injected into the vascular network, the microrobot is propelled by the blood fluid. Its uncontrolled trajectory (without magnetic force) is influenced by forces such as drag, gravity, and buoyancy exerted upon it within the vascular network. Given the frequent occurrence of bifurcations within the vascular network, controlling the microrobot's passage through these junctions is crucial to ensure its arrival at the target zone. Due to the microrobot's navigation in the vascular network, manipulating it becomes challenging in cases of high-flow velocity, such as in large-caliber arteries. To overcome this limitation, we observed that blood flow velocity varies depending on the type of vascular channel. For instance, velocity is significantly higher in the aorta and arteries, while it decreases considerably in capillaries and arterioles. Additionally, current endovascular methods utilizing catheters are highly effective for navigation in large vessels but encounter limitations when navigating small arteries where the affected target areas are located.

To address this limitation, we proposed employing a catheter to approach the target area, where fluid circulation is at a low velocity. Once near the target area, the microrobot is injected and our device takes over using our guidance method based on flux lines and magnetic force. This enables precise guidance in low-flow regions, where microrobot control becomes more feasible and efficient. Continuing our study, we focused on microrobot navigation, assuming that catheter navigation is a widely employed method in the medical field.

To achieve this goal, we proposed generating a directional magnetic force at the bifurcations. This magnetic force will guide the microrobot from the main branch to the appropriate daughter branch, enabling it to reach the desired target zone. Our strategy aimed to exploit the hydrodynamic force, which has traditionally been regarded as a navigational constraint for microrobots, by considering it as a propulsion source. This obviates the need for sophisticated trajectory tracking systems, as our objective was to navigate the microrobot towards the target branch. The hydrodynamic force was employed for microrobot propulsion, while the magnetic force was used to guide the microrobot at the bifurcations (see Figure 2).

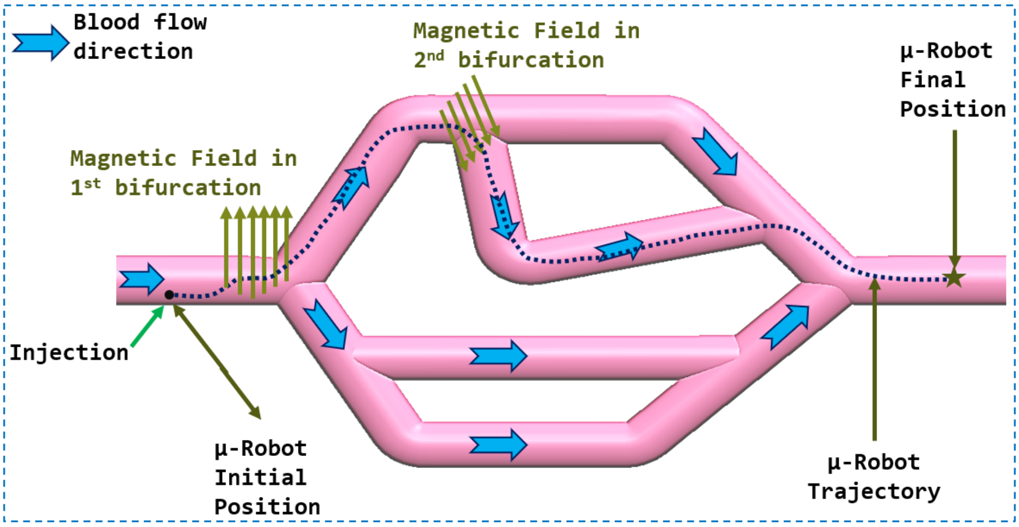

Figure 2. Diagram of the guiding strategy of a magnetic microrobot in a blood vessel by applying a magnetic field only at the bifurcation.

By adopting this approach, new perspectives are opening up in the field of microrobotic navigation, in particular to respond to the limitations of current endovasular methods. To accomplish this, we propose in this section the modeling of the microrobot's behavior within the vascular network, followed by the simulation approach for flow distribution in arteries, enabling us to gain control over velocity and hydrodynamic force. Finally, we investigated the microrobot's behavior in the presence and absence of the magnetic force, allowing for a comprehensive evaluation of its performance.

2.1. Modeling

In this study, we focused on a magnetically driven microrobot. More specifically, we chose to favor the bead-pulling strategy [27], which consists of inducing magnetic forces using magnetic field gradients. To establish effective navigation strategies, it is crucial to model the different interactions between the microrobot and the endovascular environment, allowing us to control the behavior of the microrobot.

The microrobot is modeled by a microsphere of radius R and is subjected to several vascular interaction forces, the main ones being: the hydrodynamic force F_{drag}, the gravitational force F_{gav}, the surface forces F_s (electrostatic force F_{el} and Van-der-Waals force F_{vdw}) [28].

The trajectory of a spherical microrobot in a fluid depends on all the forces described before, which can be taken into account using Newton's law given by the following expression:

$$m_p\vec{\gamma}_p = \sum \vec{F}$$

$$= \vec{F}_{mag} + \vec{F}_{drag} + \vec{F}_{gav} + \vec{F}_s. \tag{1}$$

Considering the influence of all forces (F_m, F_{drag}, F_{gav}, F_{el}, F_{vdw}) acting on a microrobot with a radius of r = 250 µm, it is evident that hydrodynamic, gravitational, and magnetic forces play prominent roles, while surface forces can be disregarded due to their negligible impact [28]. In order to simplify calculations, the remote manipulation system proposed focuses solely on the dominant forces.

Ignoring low impact forces, the total force applied on a microrobot can be expressed as follows:

$$\sum \vec{F} = \vec{F}_{mag} + \vec{F}_{drag} + \vec{F}_{gav}. \tag{2}$$

The hydrodynamic drag force is given by *Stoke's* law as:

$$F_{drag} = -6\pi\eta R(V_p - V_f), \tag{3}$$

where V_p and V_f are the microrobot and fluid velocities, respectively, R is the microrobot radius, and η is the fluid viscosity. The gravity and buoyancy force is described as follows:

$$F_{gav} = \frac{1}{6}\pi d^3(\rho_p - \rho_f)g, \tag{4}$$

where d is the microrobot diameter, g is the gravity constant, and ρ_p and ρ_f are the densities of the microrobot and blood, respectively.

The magnetic field applied to a microrobot induces a magnetic force used to steer the microrobot, this force is defined as:

$$F_m = \frac{4\pi}{3}\mu_0 R^3 M_{sat}(B)\nabla B, \tag{5}$$

where μ_0 is the permeability of free space, M_{sat} is the saturation magnetization, B is a magnetic field, and ∇B is the gradient of the magnetic field. Based on the definition of the F_m, F_{grav} and F_{drag}, the Equation (1) can be reformulated as follows:

$$m_p\gamma_p = \frac{4\pi}{3}\mu_0 R^3 M(B)\nabla B - 6\pi\eta R(V_p - V_f) + \frac{\pi d^3}{6}(\rho_p - \rho_f)g \tag{6}$$

$$m_p\begin{pmatrix}\dot{v}_x\\ \dot{v}_y\\ \dot{v}_z\end{pmatrix} = \begin{pmatrix}-6\pi\eta R(v_x - v_{f_x})\\ -6\pi\eta R(v_y - v_{f_y})\\ -6\pi\eta R(v_z - v_{f_z})\end{pmatrix} + \begin{pmatrix}0\\ 0\\ \frac{4\pi R^3}{3}(\rho - \rho_f)g\end{pmatrix} + \begin{pmatrix}f_{m_x}\\ f_{m_y}\\ f_{m_z}.\end{pmatrix} \tag{7}$$

Based on the principles described in Equation (7), the microrobot's dynamic motion can be utilized to compute its trajectory through the application of a magnetic manipulation force.

2.2. Numerical Simulation

In order to simulate the behavior of the microrobot in various scenarios, we proposed to utilize the finite element method to implement the dynamic model of the microrobot within a fluidic environment, while taking into account the desired vascular geometry. To achieve this, we exploited the Fluid–Structure Interaction (FSI) and AC/DC Magnetic modules of the COMSOL Multiphysics numerical simulation interface. Through this approach, we present the distribution of the fluid flow within the vascular network, the navigation behavior of the microrobot in multiple scenarios, as well as the validation of our navigation strategy for guiding a microrobot in bifurcations.

2.2.1. Flow Behavior in the Phantom

A vascular phantom with three successive bifurcations and variable branch diameters was modeled (see Figure 2). The objective of the first simulation was to analyze the behavior of the fluid in the vascular phantom. Therefore, the Navier–Stokes equation available in the FSI module from COMSOL Multiphysics was used. We fixed the pressure, flow, and the profile of the pulsatile velocity at the inlet of the channel as follows:

$$V_f = \overline{V_f}.(1 + a_f sin(w_f t + \phi_f)), \tag{8}$$

with $\overline{V_f}$ being the continuous component of the flow assimilated to the speed at the center of the vessel, which depends on the type of blood vessels; a_f is the amplitude of the first harmonic; w_f and ϕ_f are the pulsation and the pulsating phase shift, respectively.

Using the parameters outlined in Table 1, the outcomes of this initial simulation are depicted in Figure 3. As illustrated in Figure 3b, the velocity of flow along the walls is null due to the no-slip condition and the assumption of rigidity for the tube constituting the phantom. The flow velocity profile within the arteries exhibits a parabolic shape, with a maximum value of 12 cm/s at the center of the artery, gradually decreasing as it approaches the lateral walls. The distribution of flow within the network is influenced by both the distal pressure (see Figure 3c) and the geometry of the bifurcations (diameter and inclination angle). In this study's case, the inlet flow profile is depicted in Figure 3a, where it is evenly distributed between the two branches of the first junction. However, for the second-order bifurcation, the flow is distributed as 66% and 34% between the upper and lower branches, respectively. Finally, the lower branch of the third-order bifurcation receives 74% of the incoming flow, while the upper branch receives 26%. The relationship between flow rate and pressure enables the determination of flow velocity within each branch of the vascular network, thereby facilitating the calculation of the drag force exerted on the microrobot. This force also depends on the velocity of the microrobot, as illustrated in Figure 3d, which presents the variation of drag force as a function of flow velocity for four microrobot velocity values. It is observed that the drag force increases proportionally with flow velocity; however, as the microrobot's velocity increases, the drag force decreases until reaching equilibrium, where the microrobot's velocity matches that of the flow.

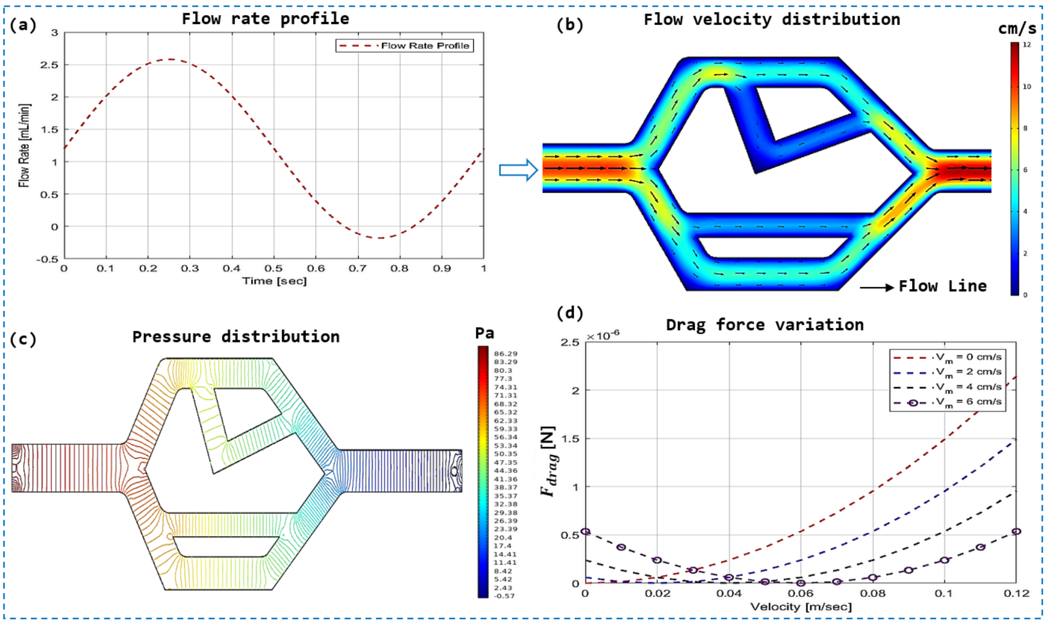

Figure 3. Simulation of fluid behavior in the vascular phantom: (**a**) flow rate profile, (**b**) flow velocity distribution, (**c**) pressure distribution, (**d**) drag force variation.

Table 1. Parameters used in the numerical simulation study.

Designation	Value
Microrobot raduis	$R = 250$ [µm]
Microrobot density	$\rho_r = 7500$ [Kg/m^3]
Microrobot volume	$V_p = \frac{4}{3}\pi R^3$ [m^3]
Fluid density	$\rho_f = 1000$ [Kg/m^3]
Fluid viscosity	$\eta = 10^{-6}$ [N·s/m^2]
Inlet pressure	$P_{inlet} = 200$ [Pa]
Fluid velocity	$\overline{V_f} = 100$ [mm/s] case of a small artery
Vacuum permeability	$\mu_0 = 1.26 \times 10^{-6}$

2.2.2. Microrobot Behavior without Magnetic Actuation

The aim of the simulations depicted in Figure 4 was to investigate the behavior of the microrobot under the influence of flow circulation, taking into account its initial position within the phantom.

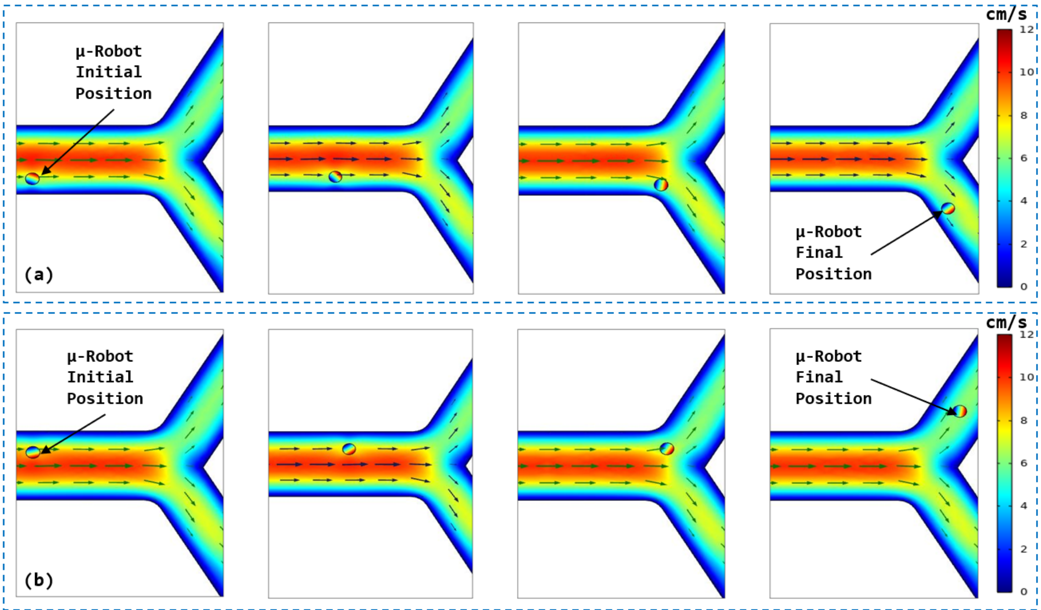

Figure 4. Trajectory of the microrobot according to its initial position in the mother artery: (**a**) microrobot positioned initially towards the lower wall of the parent artery, (**b**) microrobot positioned initially towards the upper wall of the parent artery.

The analysis of scenarios (a) and (b) in Figure 4 reveals that, when the microrobot is situated in proximity to the channel walls, it is carried by the flow towards the corresponding branch aligned with that wall. Consequently, we can conclude that the distribution and velocity of flow lines, as well as the initial positioning of the microrobot in the vascular channel, exert a significant influence on the microrobot's trajectory (see Figure 4). This is precisely what we aimed to exploit in our navigation strategy. By applying an external magnetic force, we can effectively guide the microrobot towards the region where the flow lines are directed towards the target branch.

2.2.3. Microrobot Behavior with Magnetic Actuation

Based on the numerical simulation results presented in Figure 4, we proposed a navigation strategy which consists of guiding the microrobot only at the bifurcation. For this, we employed two distinct types of magnetic forces, denoted as F_{mH} and F_{mT}. The magnetic holding force (F_{mH}) is responsible for positioning the microrobot in an area where the flow lines align with the desired branch. This force must not be overestimated to prevent the microobot from coming into contact with the wall. On the other hand, the transitional magnetic force (F_{mT}) enables the microrobot to be deflected towards the targeted branch. To guarantee safety and prevent the microrobot from going to the non-targeted branch, the force F_{mT} is greater than F_{mH}.

To validate our navigation strategy, we positioned the microrobot within the main artery of the vascular phantom and initially directed it towards the lower wall. As depicted in Figure 5, the trajectory of the microrobot without magnetic guidance is indicated in red, demonstrating its navigation following the direction of the flow lines. In contrast, we designed a distinct trajectory (in black) deviating from the microrobot's natural path. To achieve this trajectory, we employed magnetic forces in accordance with our navigation strategy. The results presented in Figure 5 demonstrate that, by applying a sustaining magnetic force (F_{mH}), the microrobot is displaced towards the upper wall where the flow lines converge towards the desired branch. Subsequently, upon reaching the bifurcation, a transitional magnetic force was applied to ensure the microrobot's passage to the intended branch. The same process was repeated for the second bifurcation until the completion of the planned trajectory.

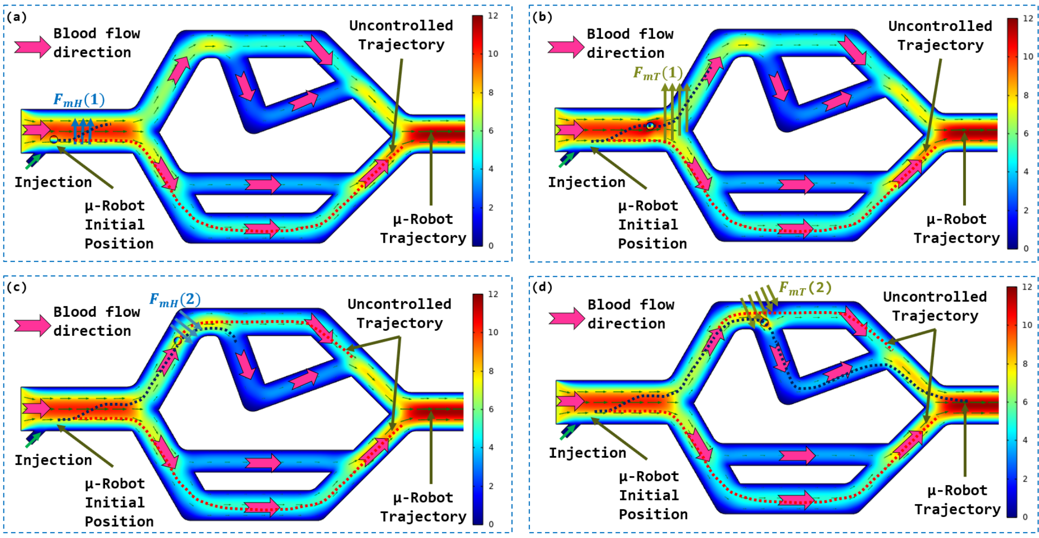

Figure 5. Numerical simulation of a microrobot in a blood vessel: (**a**) (F_{mH}) magnetic Holding Force, (**b**) (F_{mT}) transitional Magnetic Force, (**c**) navigation on the second mother artery, (**d**) magnetic navigation in the second bifurcation.

As suggested by the strategy shown in Figure 6, the magnetic force propels the microrobot towards a safe zone, which guarantees the safe passage of the bifurcation by exploiting the flow. This external force will be generated by an electromagnetic actuation system remotely controlled with a haptic device. All the components of the magnetic platform will be presented in the next section.

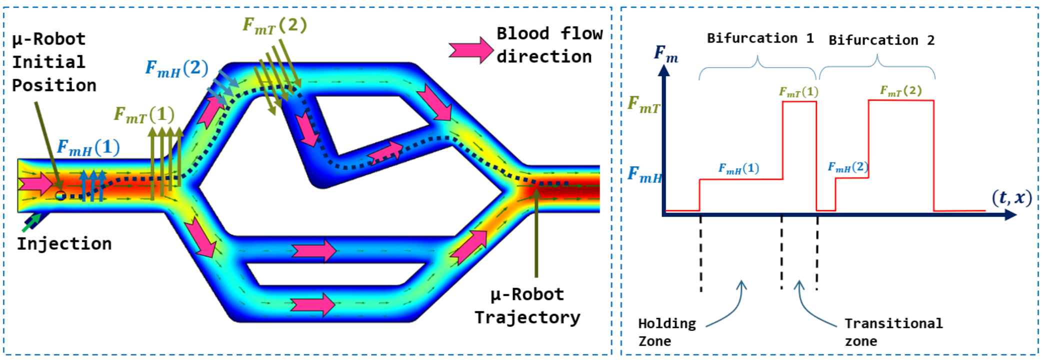

Figure 6. Guidance of the microrobot transported by the flow and actuated with a magnetic force at the bifurcations.

3. Navigation Platform Overview

3.1. Electro-Magnetic Actuation Device

To experimentally implement the proposed navigation strategy outlined in this article, we employed an electromagnetic actuation system combined with a haptic device. This choice of system enables the activation and deactivation of the magnetic field, making it suitable for medical applications. The magnetic microrobot navigation demonstrator, depicted in Figure 7, was developed in our laboratory [29]. This demonstrator consists of eight electromagnets positioned around the workspace. It was designed to generate a magnetic field of up to 0.15 Tesla on z-axis, 0.4 Tesla on x and y-axis within a central volume of 7 cm^3 by controlling the currents passing through the coils of the electromagnets. Moreover, the electromagnets incorporate soft cylindrical magnetic cores, which enhance the intensity and gradients of the magnetic field within the central region of the workspace. In particular, the soft magnetic core was chosen due to its ability to magnetize easily in the presence of an external magnetic field and rapidly demagnetize when the electrical currents are cut off. The maximum magnetic field strength (0.15 T on the z-axis, 0.4 T on the x and y-axis) generated by the eight electromagnets proved sufficient to exert the necessary forces on the microrobot, enabling efficient guidance towards the desired zone.

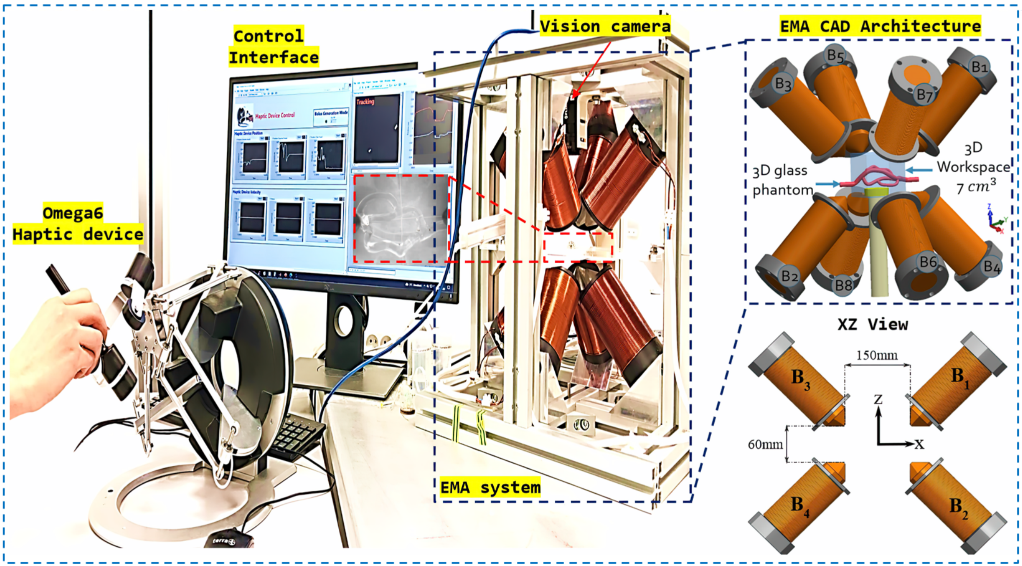

Figure 7. Microrobot manipulation platform, integrating the electromagnetic actuation system and a triaxial positioning system to position the vascular phantom in the workspace: B1/B3 (on Z+); B2/B4 (on Z−); B1/B4/B6/B7 (on X+); B2/B3/B5/B8 (on X−); B1/B4/B5/B8 (on Y+); B2/B3/B6/B7 (on Y−).

This magnetic actuation system has demonstrated remarkable navigational capabilities for magnetic microrobots in diverse environments, including the inner ear and blood vessels [29,30]. The system has been integrated into a platform comprising electronic cards and power supply units for managing the electrical currents passing through the coils. Additionally, a graphical user interface facilitates the manipulation of magnetic microrobots.

3.2. Haptic Device

As described in the introduction, our navigation strategy is based on integrating the operator (doctor) into the control loop. This aims to provide assistance during manipulation and to benefit from the skills of the doctor. This consists of using a haptic interface to convert the movements in space of the operator's hand into actions of magnetic forces to act on the movement of the microrobot remotely in its environment.

The Omega 6 haptic system, developed by Force Dimension, is a force-feedback robotic device with 6-DOF, enabling the user to perform translational and rotational movements in space. With a typical range of ±180° for rotations and 150 mm for translations, this system offers high positional accuracy, reaching levels in the micron range. Customization, control, and characterization of the Omega haptic device are described in [31]. A haptic device is typically used as a position control device in which displacement of the end-effector is directly correlated to the displacement of the avatar displayed on the screen. To integrate the haptic device into the guidance platform, we based it on the analytical model of the actuator. This model makes it possible to generate the magnetic fields in any point of the workspace:

$$H(x,y,z) = \sum_{j=1}^{8} \widetilde{H}_j(x,y,z).I_j. \tag{9}$$

$\widetilde{H}_j(x,y,z)$ is defined as the unit vector of spatial distribution, which is generated by a coil j traversed by an excitation current I_j. The calculation of the axial currents I_x, I_y and I_z can be found using the pseudo-inverse of the following equation:

$$\begin{Bmatrix} H_x \\ \\ H_y \\ \\ Hz \end{Bmatrix} = \begin{Bmatrix} f(I_x) \\ \\ f(I_y) \\ \\ f(Iz). \end{Bmatrix} \tag{10}$$

The allocation of the electric current to the different coils is carried out as follows:

$$\begin{Bmatrix} I_1 = I_4 = -I_6 = -I_7 = I_x^+ \\ -I_1 = -I_4 = I_5 = I_8 = I_y^+ \\ I_1 = I_3 = I_z^+ \end{Bmatrix}; \begin{Bmatrix} I_2 = I_3 = -I_5 = -I_8 = I_x^- \\ -I_2 = -I_3 = I_6 = I_7 = I_y^- \\ I_2 = I_4 = I_z^-, \end{Bmatrix} \tag{11}$$

where (I_x^+, I_y^+, I_z^+) and (I_x^-, I_y^-, I_z^-) are the positive and negative axial currents, respectively. The current I_j is that injected into the coil j. Equation (11) presents all the combinations of currents to navigate in 3D space using the haptic system.

To illustrate the use of the platform, we implemented an architecture to manage the interaction between the user, the haptic system, the control module, and the magnetic actuation system. This architecture is presented in Figure 8 and consists of three modules :

- Control panel module: composed of the haptic device and a user interface allowing visual feedback of the workspace and the modification of the electronic card parameters.
- Computation module: composed of an algorithm allowing the movement of the haptic device effector to be transformed into amplitude and direction of the field and magnetic force. This transformation is based on a calibration method illustrated in Figure 9, which converts the movements of the haptic device of each axis into electric currents and magnetic field. These parameters are used by the analytical model of the EMA system to calculate the electrical currents required for each coil.
- EMA module: composed of an EPOS cards box and a set of coils to generate the desired force in the workspace.

The three modules must interact to guide the microrobot in the environment. Initially, the user activates the haptic device to send the position of its effector to the calculation module. The latter makes it possible to generate the amplitude and direction of magnetic force, and the analytical model is used to calculate the electrical currents necessary for each coil. The EMA module powers the coils via electronic cards and induces a movement of the microrobot in the workspace that can be viewed in the user interface. This process is repetitive until the microrobot reaches the target area.

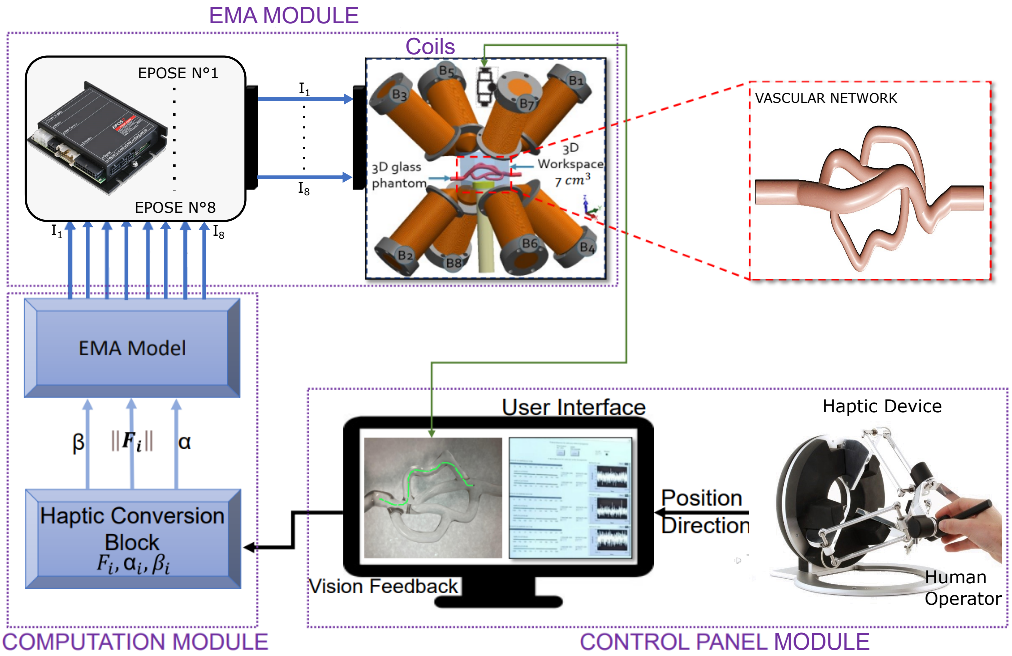

Figure 8. Magnetic actuation system control module and control interface according to the navigation strategy.

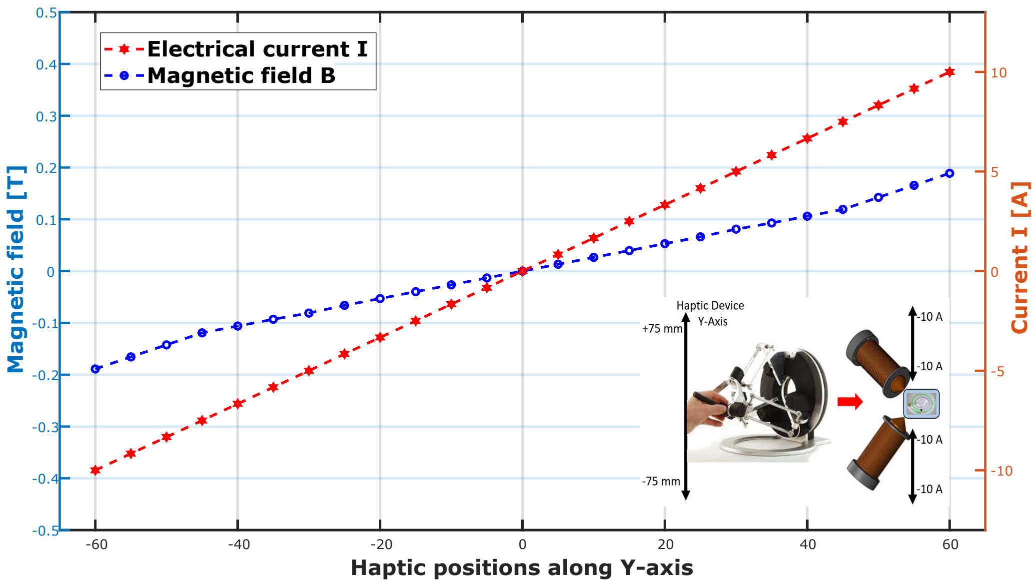

Figure 9. Conversion of the movements of the haptic system into electric current for the control of the amplitude and the direction of the magnetic field.

To ensure the correct functioning of the haptic system, we set up a calibration that allows the transformation of the positions of the axes of the haptic system into current and direction. These will generate a magnetic field of a given amplitude and direction. For this, we have presented in Figure 9 the magnetic field generated by each position of the Y axis of the haptic system. We note that, in the case where the position of the haptic is positive and maximum—the magnetic field takes the positive direction and maximum amplitude—the reverse remains true.

4. Experimental Evaluation

4.1. Haptic Control Validation

The fundamental objective of this experimentation was to validate the integration of the haptic device and demonstrate its utility in the precise manipulation of a microrobot. Indeed, the integration of the haptic device into the platform aims to enable the user to manipulate a microrobot through manual movements of the haptic joystick, while referring to the visual feedback from the vision system for synchronization. With this goal in mind, we positioned the microrobot in a free space and proceeded with manipulation using the effector of the haptic device to control the microrobot's movements.

A thorough analysis of Figure 10 reveals a close correlation between the movements of the microrobot and those of the haptic system, attesting to the fact that the manipulation of the microrobot is entirely commanded by the user through the haptic device. Notably, the user is able to reach the four target points by controlling the effector of the haptic system. This close correspondence convincingly validates the successful integration of the haptic device and confirms its capability to provide intuitive and precise control of the microrobot during manipulation operations. Remarkably, the user, unaware of it, directs the haptic system towards a specific direction, and the microrobot faithfully follows that direction. In the background, the controller generates magnetic fields by injecting electrical currents into the coils to achieve the desired trajectory.

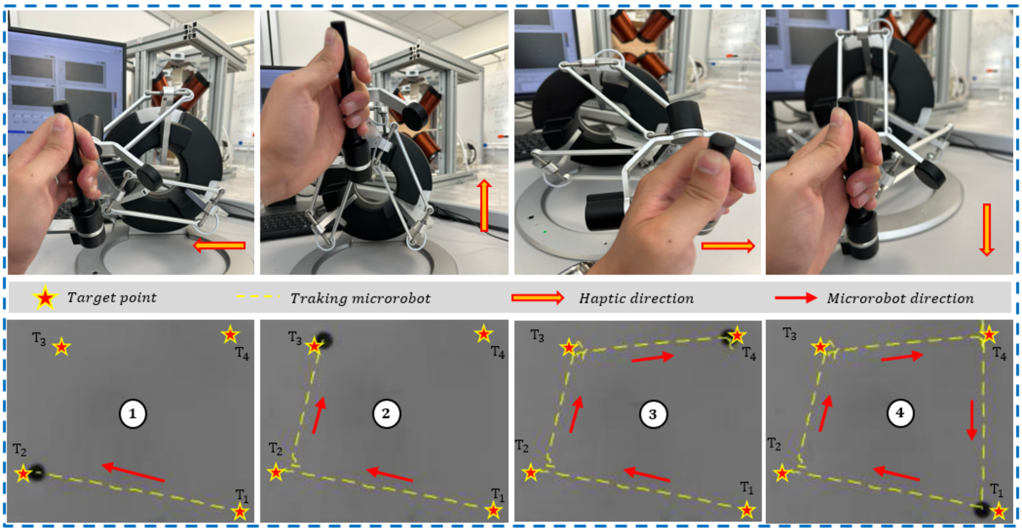

Figure 10. Validation of the microrobot control in a free space using haptic device.

4.2. Navigation Strategy Validation

In this section, two experiments were conducted to validate the proposed navigation strategy outlined in Section 2. The first experiment aimed to compare the in-silico test (presented in Figure 5) with the in-vitro test in order to corroborate the modeling of the navigation strategy and ascertain the significance of integrating a joystick for navigation purposes. The second experiment entailed validating the performance of the guidance platform within a 3D vascular network for guiding soft ferromagnetic microrobots.

In our experiments, we used a soft magnetic microrobot consisting of a microsphere made of soft iron (AISI-35C) with an average radius of 250 µm. AISI-35C is a magnetic stainless steel containing between 16 and 18% chromium and between 0.95 and 1.2% carbon. It is known for its moderate resistance to corrosion, which is particularly advantageous for medical applications. However, it should be noted that a gold coating layer should be provided in a real-life context to prevent any potential toxicity risks.

The spherical geometry imparts specific properties to the microrobot in terms of magnetic navigation. Note that our microrobot is of the soft ferromagnetic type and that its magnetization depends on the magnetic field generated by the magnetic actuation system. Since our system generates magnetic fields greater than 0.03 T, we can therefore consider its magnetization at saturation given by: $M_{sat} = \frac{B_{sat}}{\mu_0}$. To emulate the blood environment, we used a mixed solution composed of 25% glycerin and 75% water. The primary objective of these experimental tests was to validate the navigation strategy within phantoms and substantiate the efficacy of a haptic platform guiding the microrobots within the vascular network.

4.2.1. Navigation Strategy Validation in a Vascular 2D Phantom

For the initial experiment, we employ a 2D vascular network consisting of an inlet artery receiving the flow, three bifurcations with different angles, as illustrated in Figure 11, and an outlet artery connected to the reservoir. The vascular network is designed using computer-aided design (CAD) and fabricated in glass.

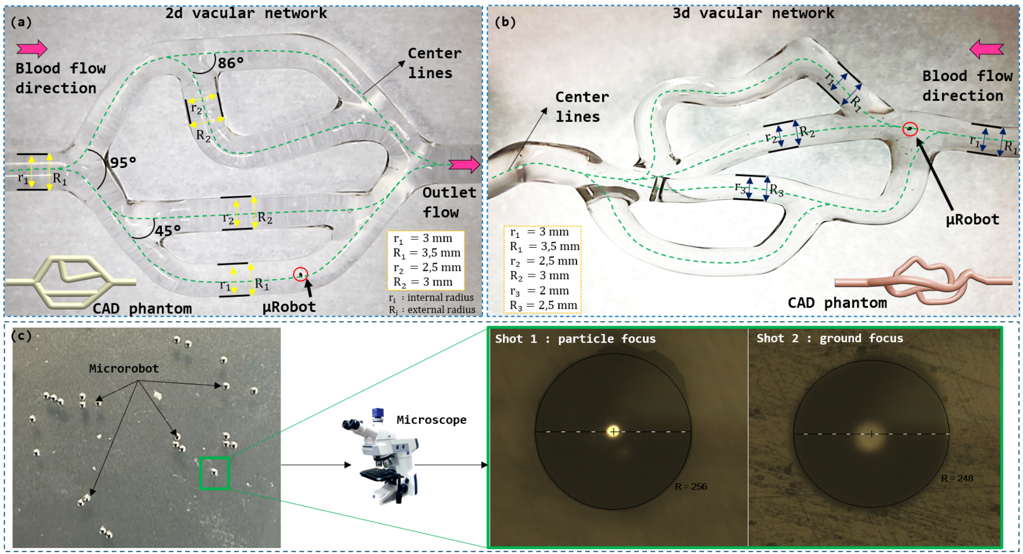

Figure 11. Vascular phantom with multi-bifurcations for microrobot navigation: (**a**) 2D vascular network; (**b**) 3D vascular network; (**c**) microrobot and their measurement under microscope.

The primary objective of this elementary experiment was twofold. Firstly, we aimed to validate the navigation strategy employing two forces through the use of a joystick, as presented in the modeling section. Secondly, we sought to verify the magnetic system's capability to generate a sufficiently strong force to guide the soft ferromagnetic microrobot. To accomplish this, we adopted navigation parameters similar to those utilized in the numerical simulation (see Table 1). The fluid's viscosity and density were fixed by adjusting the glycerin and water mixture, while the pulsatile flow was ensured by the pump. Regarding the selection of the continuous flow velocity $\overline{V}_f$, careful control of the pump-delivered flow rate $\overline{Q}_f$, the length of the conduit between the vessel inlet and the pump outlet l, the radius of this conduit R, and the pressure drop associated with this length were necessary. These parameters contribute to the following formula for calculating the flow velocity:

$$\delta P = \frac{8\eta}{\pi \cdot R^4} \overline{Q}_f \cdot l \tag{12}$$

$$\overline{V}_f = \frac{R^2}{8\eta \cdot l} \cdot \delta P. \tag{13}$$

Equation (12) was used to calculate the pressure drop between the pump outlet and the vascular network inlet, while Equation (13) was used to determine the velocity at the vessel inlet. For instance, a tube length of 10 cm and a flow rate of 72 mL/min yield a pressure drop of 0.6 mmHg, resulting in an applied velocity of 10 cm/s. In the experiment, the pump was calibrated to a flow rate of 72 mL/min.

An analysis of Figure 12 provides us with a detailed view of the magnetic-guidance-free navigation of the microrobot within the 2D vascular network device. During this initial phase, the microrobot is subjected solely to hydrodynamic force, without the intervention of an external magnetic force. This approach allowed us to observe the microrobot's uncontrolled trajectory based on its initial position. Notably, the microrobot's trajectory in Figure 12 is opposite to that in Figure 12 due to its initial position within the inlet artery.

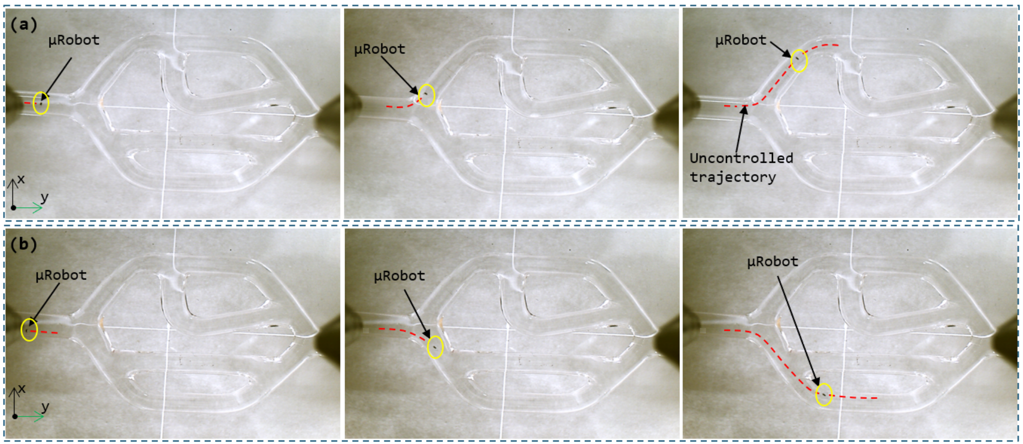

Figure 12. The uncontrolled trajectory of the microrobot in the vascular network according to different initial positions: (**a**) first trajectory, (**b**) second trajectory.

It is worth noting that, in accordance with our predictions based on numerical simulation, the microrobot's uncontrolled trajectory is closely tied to key factors such as its initial position relative to the central axis of the artery and the orientation of blood flow lines. These parameters significantly influence the direction and speed of the microrobot's movement as it navigates through the artificial vascular network. As a result, each initial configuration yields a unique trajectory. These experimental observations confirm and validate the findings obtained from the numerical model, further underscoring the significance and relevance of the proposed navigation strategy. This strategy entails combining hydrodynamic forces with magnetic guidance to achieve precise and controlled microrobot navigation within the vascular network.

We are now harnessing the magnetic force generated by the magnetic actuation system to guide the microrobot along a desired trajectory, distinct from its uncontrolled path. In the case where the microrobot is positioned at a distance of -1.4 mm from the central axis, its uncontrolled trajectory is depicted in Figure 12. To achieve the trajectory illustrated in Figure 13, it is imperative to guide the microrobot in the two bifurcations by magnetically directing it towards the first zone and the second zone, respectively, for bifurcations 1 and 2. To accomplish this, the operator manipulates the haptic joystick to generate a force of magnitude $F_{mH} = 1.35 \times 10^{-4}$ N in order to bring the microrobot back into the secure zone and prepare it for passage into the desired branch. As the microrobot reaches the entrance of the bifurcation, the operator generates a magnetic force of magnitude $F_{mT} = 4.6 \times 10^{-4}$ N to ensure a smooth transition into the desired branch. The transition between these two forces occurs continuously, with a gradual increase in magnetic force in the same direction, utilizing the haptic system's effector.

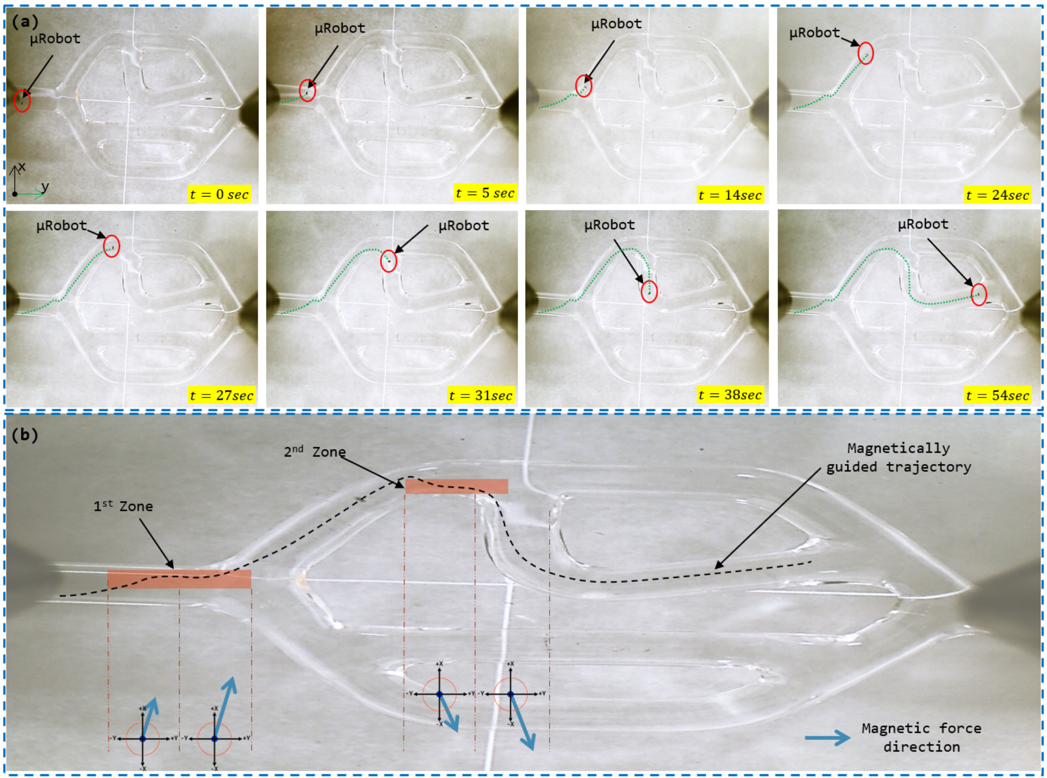

Figure 13. Microrobot trajectory in the vascular vessel subjected to the control signal applied by the user via the joystick: (**a**) Magnetically guided trajectory of the microrobot; (**b**) Directions of the magnetic forces to guide the microrobot in the two bifurcations.

4.2.2. Navigation Strategy Validation in a Vascular 3D Phantom

The objective of this experiment was to demonstrate the navigation capability of a soft ferromagnetic microrobot through a 3D vascular model. The model used, as depicted in Figure 11, simulates the dimensions of small arteries and arterioles, with diameters ranging from 2 to 3 mm.

The experiment (shown in Figure 14) aims to validate the performance of our magnetic actuation platform for 3D guidance. Initially, we assessed the microrobot's uncontrolled trajectory within the vascular network, as illustrated in Figure 14. Based on these findings, we planned a magnetic guidance trajectory to control the microrobot through two successive bifurcations.

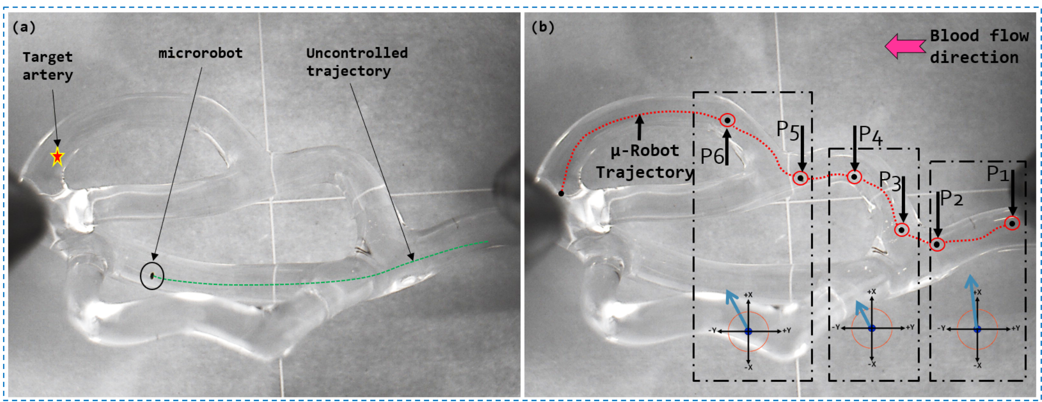

Figure 14. Magnetic guidance result of a soft ferromagnetic microrobot in a 3D vascular network: (**a**) Non-magnetic trajectory; (**b**) Magnetic guidance trajectory.

In accordance with the previously established navigation strategy, we employed a magnetic force $F_{mH} = [F_{mH}(x); F_{mH}(y); 0]$ applied in the (O, x, y) plane to deviate the microrobot from its natural trajectory. In the subsequent phase, a transition force $F_{mT} = [F_{mT}(x); 0; F_{mT}(z)]$ was generated in the (O, x, z) plane, allowing the microrobot to precisely penetrate into the desired first branch. To reach the final destination, a magnetic force was applied to facilitate the smooth transition of the microrobot through the second branch, thereby counteracting its tendency to continue along its uncontrolled trajectory.

The magnetic guidance platform, based on the analysis of control signals and the results of this experiment, provides the capability to generate a three-dimensional magnetic force within the range of $[-1.13 \;\; 1.13] \times 10^{-3}$ N for a soft ferromagnetic particle with a diameter of 250 µm. The navigation strategy employing two forces, F_{mH} and F_{mT}, facilitated by the use of a haptic joystick, enhances navigation simplicity and effectiveness.

In order to ensure the comprehensive evaluation of the magnetic navigation platform's performance, it is important to investigate the effect of flow velocity variation on the navigation efficacy. With this objective in mind, we conducted the same magnetic guidance test as depicted in Figure 14 at different flow velocities. These velocities were determined by employing Equations (12) and (13). The pump generated flow rates to simulate velocities ranging from 30 to 150 mL/min. The results depicted in the Figure 15 reveal that the magnetic navigation performance is significantly influenced by the flow velocity. Specifically, at lower flow velocities in the range of 1 to 4 cm/s, the success rate reaches 100%. However, as the flow velocity is increased to between 8 and 12 cm/s, the success rate declines to a range of 80% to 20%. Beyond 14 cm/s, complete control over the microrobot is lost.

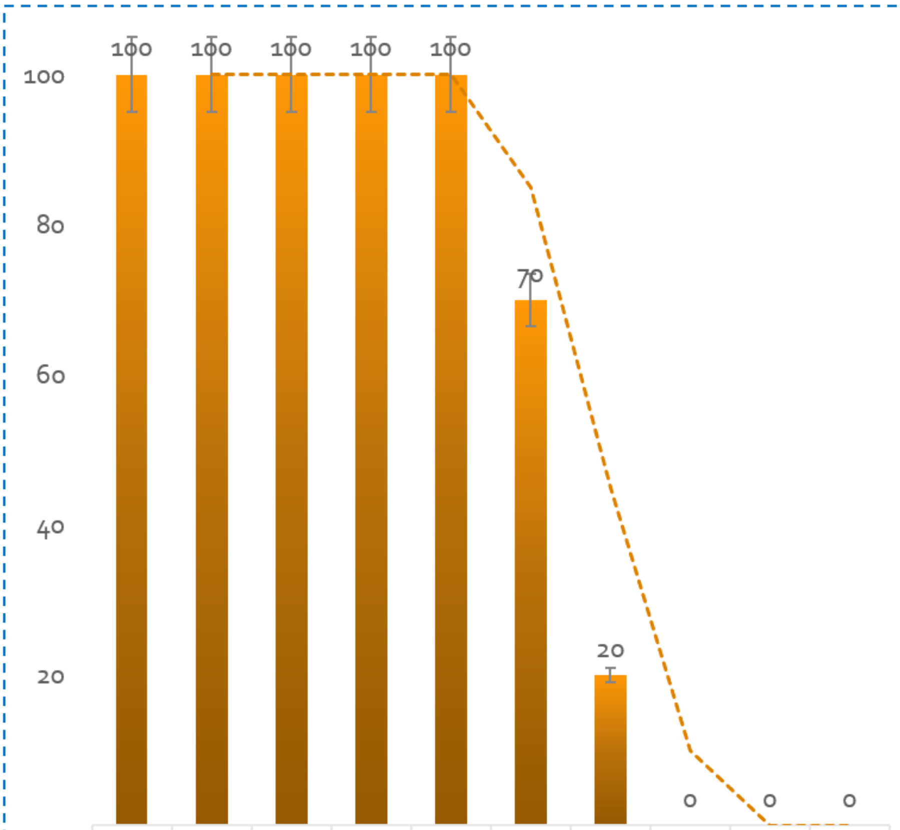

V_f	1	2	4	6	8	10	12	14	16	18
%	100	100	100	100	100	70	20	0	0	0

Figure 15. Success rate of microrobot guidance at different flow velocity values. The results are calculated on an average of 10 tests per speed.

5. Conclusions

This article described the development of a navigation strategy for a soft magnetic microrobot, implemented by means of a haptic system integrated with a magnetic actuation platform designed in our research laboratory. We demonstrated, through numerical simulations carried out on an in silico model, the feasibility of exploiting the hydrodynamic forces of the flow to guide the microrobot by combining them with the magnetic forces. Indeed, these hydrodynamic forces, long perceived as an obstacle to navigation, can help us transport the microrobot and reduce the need to use magnetic forces, except at bifurcations, to guide the microrobot towards the target artery. With this in mind, our simulations also demonstrated that the navigation of the microrobot strongly depends on its initial position in the main artery.

To generate magnetic forces, we used our magnetic guidance platform, composed of electromagnetic coils, which has proven its effectiveness for the navigation of microrobots in various environments of the human body. This platform has been adapted by integrating a haptic system in order to involve the user in the control loop, thus making it possible to benefit from the expertise of the surgeon and to facilitate navigation. To demonstrate the efficiency of the proposed magnetic actuation system, we performed microrobot control experiments in two vascular networks. The first network was in 2D and made it possible to validate in-silico navigation results with and without magnetic actuation force. The second network, in 3D, demonstrated the effectiveness of the navigation procedure in more complex bifurcations. In the first network, the microrobot was successfully guided through two consecutive bifurcations in 10 trials, achieving a 100% success rate for flow velocities below 8 cm/s. This demonstrates the effectiveness of our method in successfully navigating vascular network bifurcations. For the complex 3D vascular network with pronounced curvatures, navigation results showed good control of the microrobot in traversing the bifurcations. However, when conducting varied tests with flow velocities ranging from 1 to 10 cm/s and repeating each test 10 times, the observed success rate was 59%. These results highlight the challenges associated with navigation in complex vascular networks, but still demonstrate adequate control of the microrobot under low-flow conditions. As specified in the navigation strategy section, our method was designed with the understanding that microrobots will primarily operate in arteries with relatively low-flow velocities. This is made possible by using endovascular catheters that facilitate access to these areas. Thus, our magnetic-guidance method specifically addresses the limitations of conventional endovascular methods, making it a relevant strategy in the clinical context. It provides a complementary solution for precise navigation in complex vascular networks and for reaching specific target areas.

Through these experimental tests, the guidance strategy with a haptic system has demonstrated its ability to offer simple and intuitive magnetic navigation to reach specific areas of the vascular network. Our future studies will include improving the current magnetic platform in several ways, such as developing a human-scale magnetic actuation system to increase workspace and enable in-vivo testing, taking into account medical constraints. We also plan to improve the haptic system by integrating force feedback to interact with the walls (in particular to control the F_{mh} force). As for limiting the navigation of microrobots to velocities above 100 mm/s, the approach proposed in this article can be easily implemented in low-velocity arteries such as liver and kidney, where flow velocities are well below 100 mm/s. From the same perspective, we aim to maximize the use of haptic devices for full integration of the clinician in the procedure. The envisioned improvement is the utilization of force feedback in the haptic device, enabling the operator to feel the magnetic force during microrobot's manipulation. We plan to incorporate magnetic force limitation modules to prevent undesirable interactions with surrounding tissues. For future developments, we intend to create a virtual environment that integrates the vascular network based on medical images and is fed in real-time by physiological data of blood circulation. This approach would reduce reliance on real-time medical images, thereby minimizing X-ray exposure time for both patients and operating room personnel.

Author Contributions: Conceptualization, All authors; methodology, All authors; software, A.C.; formal analysis, All authors; investigation, A.C.; resources, K.B.; data curation, A.C.; writing original draft preparation, All authors; writing review and editing, All authors; visualization, All authors; supervision, K.B.; project administration, K.B.; funding acquisition, K.B. All authors have read and agreed to the published version of the manuscript.

Funding: This work was supported by µ-Mag project, founded by Junia-HEI campus centre, in France.

Data Availability Statement: Data are available from the corresponding author on request.

Conflicts of Interest: The authors declared no potential conflict of interest with respect to the research, authorship, and/or publication of this article.

References

1. Steichen, S.D.; Caldorera-Moore, M.; Peppas, N.A. A review of current nanoparticle and targeting moieties for the delivery of cancer therapeutics. *Eur. J. Pharm. Sci.* **2013**, *48*, 416–427. [CrossRef] [PubMed]
2. Bar, J.; Herbst, R.S.; Onn, A. Targeted drug delivery strategies to treat lung metastasis. *Expert Opin. Drug Deliv.* **2009**, *6*, 1003–1016. [CrossRef] [PubMed]
3. Nelson, B.J.; Kaliakatsos, I.K.; Abbott, J.J. Microrobots for minimally invasive medicine. *Annu. Rev. Biomed. Eng.* **2010**, *12*, 55–85. [CrossRef] [PubMed]
4. Flynn, A.; Udayakumar, K.; Barrett, D.; McLurkin, J.; Franck, D.; Shectman, A. Tomorrow's surgery: Micromotors and microrobots for minimally invasive procedures. *Minim. Invasive Ther. Allied Technol.* **1998**, *7*, 343–352. [CrossRef]
5. Ullrich, F.; Bergeles, C.; Pokki, J.; Ergeneman, O.; Erni, S.; Chatzipirpiridis, G.; Pané, S.; Framme, C.; Nelson, B.J. Mobility experiments with microrobots for minimally invasive intraocular surgery. *Investig. Ophthalmol. Vis. Sci.* **2013**, *54*, 2853–2863. [CrossRef]
6. Hamdi, M.; Ferreira, A. Guidelines for the design of magnetic nanorobots to cross the blood–brain barrier. *IEEE Trans. Robot.* **2013**, *30*, 81–92. [CrossRef]
7. Nacev, A.; Beni, C.; Bruno, O.; Shapiro, B. The behaviors of ferromagnetic nano-particles in and around blood vessels under applied magnetic fields. *J. Magn. Magn. Mater.* **2011**, *323*, 651–668. [CrossRef]
8. Jing, X.; Guo, W. Modeling and Configuration Design of Electromagnetic Actuation Coil for a Magnetically Controlled Microrobot. *Chin. J. Mech. Eng.* **2019**, *32*, 63. [CrossRef]
9. Petruska, A.J.; Mahoney, A.W.; Abbott, J.J. Remote manipulation with a stationary computer-controlled magnetic dipole source. *IEEE Trans. Robot.* **2014**, *30*, 1222–1227. [CrossRef]
10. Go, G.; Choi, H.; Jeong, S.; Lee, C.; Ko, S.Y.; Park, J.O.; Park, S. Electromagnetic navigation system using simple coil structure (4 coils) for 3-D locomotive microrobot. *IEEE Trans. Magn.* **2014**, *51*, 1–7.
11. Jeong, S.; Choi, H.; Choi, J.; Yu, C.; Park, J.o.; Park, S. Novel electromagnetic actuation (EMA) method for 3-dimensional locomotion of intravascular microrobot. *Sens. Actuators A Phys.* **2010**, *157*, 118–125. [CrossRef]
12. Kratochvil, B.E. ; Kummer, M.P.; Abbott, J.J.; Borer, R.; Ergeneman, O.; Nelson, B.J. Octomag: An electromagnetic system for 5-dof wireless micromanipulation. *IEEE Trans. Robot.* **2010**, *26* , 1006–1017
13. Niu, F.; Ma, W.; Chu, H.K.; Ji, H.; Yang, J.; Sun, D. An electromagnetic system for magnetic microbead's manipulation. In Proceedings of the 2015 IEEE International Conference on Mechatronics and Automation (ICMA), Beijing, China, 2–5 August 2015; IEEE: Piscataway, NJ, USA , 2015; pp. 1005–1010.
14. Pawashe, C.; Floyd, S.; Sitti, M. Modeling and experimental characterization of an untethered magnetic micro-robot. *Int. J. Robot. Res.* **2009**, *28*, 1077–1094. [CrossRef]
15. Floyd, S.; Pawashe, C.; Sitti, M. An untethered magnetically actuated micro-robot capable of motion on arbitrary surfaces. In Proceedings of the 2008 IEEE International Conference on Robotics and Automation, Pasadena, CA, USA, 19–23 May 2008; IEEE: Piscataway, NJ, USA, 2008; pp. 419–424.
16. Diller, E.; Giltinan, J.; Lum, G.Z.; Ye, Z.; Sitti, M. Six-degree-of-freedom magnetic actuation for wireless microrobotics. *Int. J. Robot. Res.* **2016**, *35*, 114–128. [CrossRef]
17. Pacchierotti, C.; Magdanz, V.; Medina-Sánchez, M.; Schmidt, O.G.; Prattichizzo, D.; Misra, S. Intuitive control of self-propelled microjets with haptic feedback. *J. Micro-Bio Robot.* **2015**, *10*, 37–53. [CrossRef]
18. Hamdipoor, V.; Afzal, M.R.; Le, T.A.; Yoon, J. Haptic-based manipulation scheme of magnetic nanoparticles in a multi-branch blood vessel for targeted drug delivery. *Micromachines* **2018**, *9*, 14. [CrossRef] [PubMed]
19. van West, E.; Yamamoto, A.; Higuchi, T. The concept of "Haptic Tweezer", a non-contact object handling system using levitation techniques and haptics. *Mechatronics* **2007**, *17*, 345–356. [CrossRef]
20. Pacoret, C.; Regnier, S. Invited article: A review of haptic optical tweezers for an interactive microworld exploration. *Rev. Sci. Instruments* **2013**, *84*, 081301. [CrossRef]
21. Basdogan, C.; Kiraz, A.; Bukusoglu, I.; Varol, A.; Doğanay, S. Haptic guidance for improved task performance in steering microparticles with optical tweezers. *Opt. Express* **2007**, *15*, 11616–11621. [CrossRef]

22. Mehrtash, M.; Tsuda, N.; Khamesee, M.B. Bilateral macro–micro teleoperation using magnetic levitation. *IEEE/ASME Trans. Mechatronics* **2011**, *16*, 459–469. [CrossRef]
23. Okamura, A.M. Methods for haptic feedback in teleoperated robot-assisted surgery. *Ind. Robot. Int. J.* **2004**, *31*, 499–508 [CrossRef]
24. Ammi, M.; Ferreira, A. Robotic assisted micromanipulation system using virtual fixtures and metaphors. In Proceedings of the Proceedings 2007 IEEE International Conference on Robotics and Automation, Rome, Italy, 10–14 April 2007; IEEE: Piscataway, NJ, USA, 2007; pp. 454–460.
25. Bolopion, A.; Xie, H.; Haliyo, D.S.; Régnier, S. Haptic teleoperation for 3-D microassembly of spherical objects. *IEEE/ASME Trans. Mechatron.* **2010**, *17*, 116–127. [CrossRef]
26. Ghanbari, A.; Horan, B.; Nahavandi, S.; Chen, X.; Wang, W. Haptic microrobotic cell injection system. *IEEE Syst. J.* **2012**, *8*, 371–383. [CrossRef]
27. Lee, S.; Kim, S.; Nelson, B.J.; Choi, H. Fabrication and targeted particle delivery using microrobots. In Proceedings of the 2015 12th International Conference on Ubiquitous Robots and Ambient Intelligence (URAI), Goyang, Republic of Korea, 28–30 October 2015; IEEE: Piscataway, NJ, USA, 2015; pp. 524–525.
28. Mellal, L.; Belharet, K.; Folio, D.; Ferreira, A. Optimal structure of particles-based superparamagnetic microrobots: Application to MRI guided targeted drug therapy. *J. Nanopart. Res.* **2015**, *17*, 1–18. [CrossRef]
29. Chah, A.; Kroubi, T.; Belharet, K. A new electromagnetic actuation system with a highly accessible workspace for microrobot manipulation. In Proceedings of the 2020 IEEE/ASME International Conference on Advanced Intelligent Mechatronics (AIM), Boston, MA, USA, 6–9 July 2020; IEEE: Piscataway, NJ, USA, 2020; pp. 723–728.
30. Chah, A.; Elfakir, H.; Meziane, L.; Belharet, K. Soft ferromagnetic microrobot navigation in the cochlea using haptic assistance. In Proceedings of the 2022 IEEE/ASME International Conference on Advanced Intelligent Mechatronics (AIM), Sapporo, Japan, 11–15 July 2022; IEEE: Piscataway, NJ, USA, 2022; pp. 626–631.
31. Ceccacci, S.; Generosi, A.; Leopardi, A.; Mengoni, M.; Mandorli, F. The role of haptic feedback and gamification in virtual museum systems. *J. Comput. Cult. Herit. (JOCCH)* **2021**, *14*, 1–14. [CrossRef]